ELSEVIER

Physica A 216 (1995) 199–212

PHYSICA A

Simulation of rotating drum experiments using non-circular particles

Volkhard Buchholtz [a,1], Thorsten Pöschel [b,2], Hans-Jürgen Tillemans [c,d,3]

[a] *Humboldt-Universität zu Berlin, Institut für Physik, Unter den Linden 6, D-10099 Berlin, Germany*

[b] *Arbeitsgruppe Nichtlineare Dynamik, Universität Potsdam, Am Neuen Palais, D-14415 Potsdam, Germany*

[c] *Höchstsleistungsrechenzentrum, Forschungszentrum Jülich, D-52425 Jülich, Germany*

[d] *Universität zu Köln, Institut für Theoretische Physik, Zülpicher Str. 77, D-50997 Köln, Germany*

Received 20 January 1995; revised 1 February 1995

Abstract

We investigate the flow of granular material in a rotating cylinder numerically using molecular dynamics in two dimensions. The particles are described by a new model which allows to simulate geometrically complicated shaped grains. The results of the simulation agree significantly better with experiments than the results which are based on circular particles.

1. Introduction

The flow of granular material in a rotating cylinder or drum reveals many interesting effects and has been studied by physicists experimentally as well as theoretically in various articles. Moreover, the knowledge of the dynamics of the material is of high interest in engineering since many important technological processes are based on the movement of granular material in rotating cylinders, such as mixing and milling (see e.g. [1–3]).

Nakagawa used magnetic resonance imaging (MRI, NMR) to observe mustard seeds moving in a rotating drum [4]. Seeds are suited because their oil contains free protons which are necessary for this method. The velocity and the concentration of the seeds in the drum could be determined very elegantly with this method. Woodle and Munro [5]

[1] E-mail: volkhard@itp02.physik.hu-berlin.de.

[2] E-mail: thorsten@hlrsun.hlrz.kfa-juelich.de.

[3] E-mail: hjt@hlrsun.hlrz.kfa-juelich.de.

SSDI 0378-4371(95)00045-3

and Rajchenbach [6] found experimentally a hysteresis for the transition from stick–slip motion of the particles to continuous motion when changing the rotation velocity of a rotating drum. There are two different critical angular velocities which separate the regimes of stick–slip and continuous flow. If the rotation frequency is increased the critical angular velocity is higher than in the case of decreasing frequency. Rajchenbach found experimentally that the relation between the surface current J, which is proportional to the angular velocity of the rotating drum, and the surface angle of the granular medium Θ obeys a power law [6]:

$$J \sim (\Theta - \Theta_c)^m. \tag{1}$$

For the exponent m they measured a value of about 0.5. Rolf and Rothkegel used a very interesting and sophisticated experimental setup to examine the collision frequency between particles in a rotating drum [1,2]. Some of the particles contained equipment for pressure measuring and microelectronic devices to store the data or transmitters to transmit the data to an external computer. Several regions with different collision rates were found.

Presently there are two different methods available for the numerical simulations of these effects.

(i) A method which is based on a model by Visscher and Bolsterli [7] was introduced in 1992 by Jullien et al. to examine a shaken granular medium [8]. Here the dynamics of the particles is calculated separately for each particle. In the case of the shaken box the particles are ordered according to their distance from the bottom of the box. Then one calculates the motion of the particles beginning with the one which has the lowest distance to the bottom while all other particles are fixed. The particle moves until it reaches a local minimum where it gets stuck. Then one calculates the next particle while all others are at fixed positions and so on. This method is very fast but it has the disadvantage that inertia and elasticity are neglected and only particles with a restitution coefficient of zero can be simulated. For this reason the model has been attacked in Ref. [9]. Nevertheless under certain conditions this model is able to reproduce the experimental behavior correctly. With a model which is based on the same method Baumann et al. found an interesting phenomenon which is also measured experimentally [10–12]: Two sorts of circular particles, originally perfectly mixed, will decompose after only one or two rotations of the drum. The smaller disks gather themselves in the center of the drum.

(ii) There are several models for the simulation of the dynamics of granular material using the molecular dynamics concept (e.g. [13]). Most of the authors apply a model introduced by Cundall and Strack [14] and Haff and Werner [15] where it is assumed that the particles are ideal circular disks i with radii R_i which interact when they touch each other. If the distance between their centers r_i is smaller than the sum of their radii they feel a repulsive force. To be able to capture the loss of energy and to simulate a restitution coefficient this movement is damped.

Hence the particles feel a force $\boldsymbol{F}_{ij}$ with the normal component F_{ij}^N and the shear component F_{ij}^S

$$\boldsymbol{F}_{ij} = F_{ij}^N \cdot \frac{\boldsymbol{r}_i - \boldsymbol{r}_j}{|\boldsymbol{r}_i - \boldsymbol{r}_j|} + F_{ij}^S \cdot \begin{pmatrix} 0 & -1 \\ 1 & 0 \end{pmatrix} \frac{\boldsymbol{r}_i - \boldsymbol{r}_j}{|\boldsymbol{r}_i - \boldsymbol{r}_j|} \tag{2}$$

with

$$F_{ij}^N = Y \cdot \left(|\boldsymbol{r}_i - \boldsymbol{r}_j| - R_i - R_j\right)^{3/2} - m_{ij}^{eff} \cdot \gamma_N \cdot v_{rel}^N, \tag{3}$$

$$F_{ij}^S = -\min(m_{ij}^{eff}\gamma_S|v_{rel}^S|, \mu|F_{ij}^N|), \tag{4}$$

$$\boldsymbol{v}^{rel} = \boldsymbol{v}_j - \boldsymbol{v}_i, \tag{5}$$

$$m_{ij}^{eff} = \frac{m_i \cdot m_j}{m_i + m_j}, \tag{6}$$

with the Young modulus Y, the damping coefficients γ_N and γ_S and the Coulomb friction coefficient μ. Eq. (5) describes the relative velocity of the surfaces of the particles at the point of contact and Eq. (6) gives the effective mass. Eq. (4) takes the Coulomb friction law into account, saying that two particles slide on top of each other if the shear force overcomes μ times the normal force. Eq. (3) comes from the Hertz law [16] for the force between two rigid bodies which are in contact with each other. This model has been applied to simulations of rotating drums by several authors. Ristow investigated the particle size segregation in a rotating drum in two dimensions [17,18], Pöschel and Buchholtz investigated the irregularities of the particle stream [19].

There are some models to simulate more complex shaped grains which are composed of circular disks. In the model by Gallas and Sokołowski [20] the grains consist of two disks connected with each other by a stiff bar. Walton and Braun used a three dimensional MD simulation with spheres and with more complicated two-dimensional particles consisting of four or eight circular disks rigidly connected with each other [21]. With this model they examined the transition from stationary to sliding and the transition from sliding to raining flow in a rotating drum. Pöschel and Buchholtz [22,23] describe grains built up of five circular disks where one of them is located in the center of the grain and four identical disks are at the corners of a square. Each pair of neighboring disks is connected by a damped spring. The latter model was applied to the rotating cylinder [19] and it was shown that the simulation results agree much better with the experiment than equivalent simulations using circular disks. Especially it was shown that one can reproduce stick–slip motion and avalanches which was not possible with circles. The inclination and the dependency of the inclination on the angular velocity, however, did not agree well with the experiment.

Another model for non-circular grains has been proposed by Mustoe and DePorter [24]. There the boundary geometry of the particles is defined (in local coordinates) by

$$f_i(x_i, y_i) = \left[\frac{|x_i|}{a_i}\right]^{n_i} + \left[\frac{|y_i|}{b_i}\right]^{n_i} - 1 = 0. \tag{7}$$

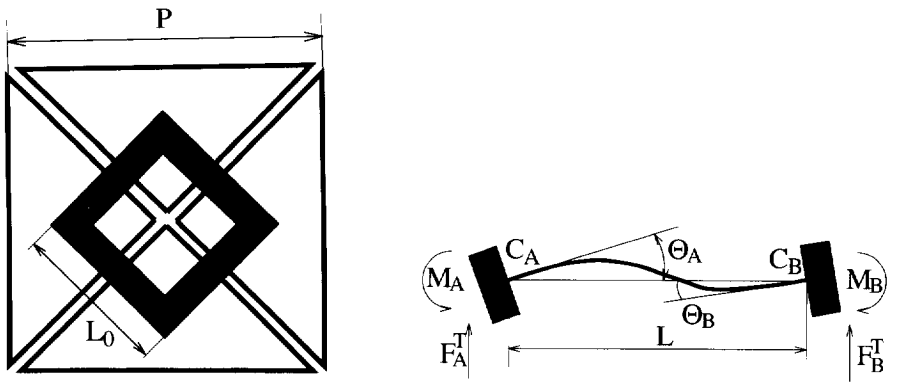

Fig. 1. Draft of a complex particle (left). The four triangles are connected by damped leaf springs as shown in the right figure. The beams are fixed at the centre of mass points of the triangles C_A and C_B. When the triangles undergo collisions the beams are elongated and bent. They disspipate energy proportionally to the deformation rate.

By changing n_i from 2 to ∞ the shape of the particles varies continuously from elliptical to rectangular. They use a complicated algorithm to detect collisions between particles. Hogue and Newland [25] investigate the flow of granular material on an inclined chute and through a hopper using a model where the boundary of the convex particles is given by a polygon with up to 24 vertices. To detect whether two particles touch each other one has to calculate the intersections between each pair of vertices. During collisions energy is dissipated according to Stronge's energy dissipation hypothesis [26] in normal direction, whilst Coulomb's friction law models the energy losses in tangential direction.

Using grains which consist of interconnected circles or of particles described by Eq. (7) it is not possible to simulate particles with sharply formed corners. For some effects it seems to be essential to simulate such particles to reproduce the experimental observed effects. This point is discussed in detail in [23,27,28]. In this paper we present molecular dynamics simulations where the particles are simulated using a more sophisticated model.

2. The model

The particles in our simulation consist of four triangles which are connected by beams of length $L_0 = P \cdot \frac{\sqrt{2}}{3}$ to simulate a square particle of side length P as shown in Fig. 1 (left). The ends of the beam are fixed at the center of mass point of the connected triangles in the direction in perpendicular to the neighboring sides of the triangles when the grain is in its rest state, i.e. no forces are applied. The beams are shadowed in Fig. 1. A beam in our sense is an elastic bar which is subjected to forces in the direction of its axis and transverse to its axis, i.e. to normal and shear forces, and to torques acting on its ends. During its deformation a beam dissipates energy similar to a linearly damped spring, i.e. proportional to its deformation rate.

The deformation of a beam between the triangles A and B with centre of mass points C_A and C_B is completely described by the angles Θ_A and Θ_B and by its length L (see Fig. 1, right). A deformed beam acts on the triangles with the torques

$$M_A = \frac{4EI}{L}\,\Theta_A + \frac{2EI}{L}\,\Theta_B, \tag{8}$$

$$M_B = \frac{2EI}{L}\,\Theta_A + \frac{4EI}{L}\,\Theta_B, \tag{9}$$

and with the forces in perpendicular to $\overline{C_A C_B}$

$$F_A^T = \frac{6EI}{L^2}\,(\Theta_A + \Theta_B)\,, \tag{10}$$

$$F_B^T = -\frac{6EI}{L^2}\,(\Theta_A + \Theta_B)\,, \tag{11}$$

where I is the moment of inertia of the beam and E is the elastic constant of the beam material. In the case of a beam with rectangular cross section of side lengths S and unity one finds

$$I = \tfrac{1}{12}S^3. \tag{12}$$

In the direction of $\overline{C_A C_B}$ the beam acts with the forces

$$F_A^N = E \cdot (L - L_0)\,, \tag{13}$$

$$F_B^N = -E \cdot (L - L_0)\,, \tag{14}$$

$$L_0 = \frac{\sqrt{2}}{3}\,P. \tag{15}$$

The torques and forces given by Eqs. (8)–(14) are valid for small deformations of the beam, i.e. we assume a linear superposition of all forces and torques [29]. For a detailed derivation of the formulae see [30].

The deformation of the beams is damped proportionally to the deformation rates

$$M_A^{(d)} = -\frac{\gamma I}{L}\,\dot{\Theta}_A, \tag{16}$$

$$M_B^{(d)} = -\frac{\gamma I}{L}\,\dot{\Theta}_B, \tag{17}$$

$$F_A^{N(d)} = -\gamma\left[v_A \cdot \overrightarrow{C_A C_B} - v_B \cdot \overrightarrow{C_A C_B}\right], \tag{18}$$

$$F_B^{N(d)} = \gamma\left[v_A \cdot \overrightarrow{C_A C_B} - v_B \cdot \overrightarrow{C_A C_B}\right], \tag{19}$$

where γ is the damping coefficient of the beam material. As mentioned above the deformation of the beam is in linear approximation completely determined by the angles Θ_A and Θ_B and the length L. Hence there is no damping force acting in shear direction.

When two triangles of *different* grains touch each other (Fig. 2), i.e. if there is an overlap between both they feel a force in perpendicular to the line between the

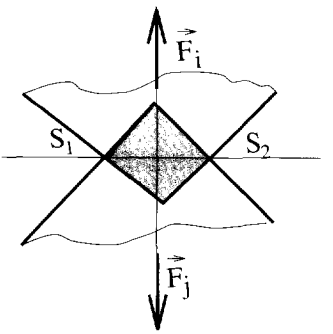

Fig. 2. According to the Poisson hypothesis the force between two interacting particles is directed in perpendicular to the intersection line $\overline{S_1 S_2}$.

intersection points $\overline{S_1 S_2}$ according to the Poisson hypothesis [31]. The absolute value of the force is assumed to be proportional to the intersection area Q times Young modulus Y

$$\left|F_A^{is}\right| = Y\, Q\ . \tag{20}$$

We want to point out that during the collision of the triangles the energy is conserved. The method is described in more detail in [30].

Adding up all forces and torques described above one finds the net forces and torques acting upon each particle. The dynamics of the grains will then be calculated by a molecular dynamics scheme (see e.g. [13]). We have chosen a Gear predictor corrector method of 5th order [32]. A beam model very similar to ours is described in detail in [33].

3. The experimental setup

Throughout our simulations we used square particles of side length P consisting of four triangles as shown in Fig. 1 where P is equally distributed in the interval $P \in [0.1\,\mathrm{cm}; 0.2\,\mathrm{cm}]$. The Young modulus Y of the material is $Y = 2 \cdot 10^7\,\mathrm{g \cdot cm^{-1} \cdot s^{-2}}$. Each connection between the triangles consists of beams with elastic constant of the beam material $E = 10^5\,\mathrm{g \cdot s^{-2}}$ and damping constant $\gamma = 5\,\mathrm{g \cdot s^{-1}}$. The moment of inertia of the beam was $I = 10^{-4}\,\mathrm{cm^3}$. When simulating relatively stiff beams we need a very small time step δt for the integration of the equations of motion to guarantee numerical stability, and hence the simulation becomes inefficient. An alternative method is to simulate each beam by two identical beams of lower elastic constant E and using a larger time step for the integration. We found that the latter approach works more efficiently. The parameters have been chosen to give the best agreement of the numerical simulated grain movement with the typical behavior of granular media. We generated an animated sequence of snapshots of the simulation and compared the behavior of the granular material with what we would expect from a real material. The cylinder had a

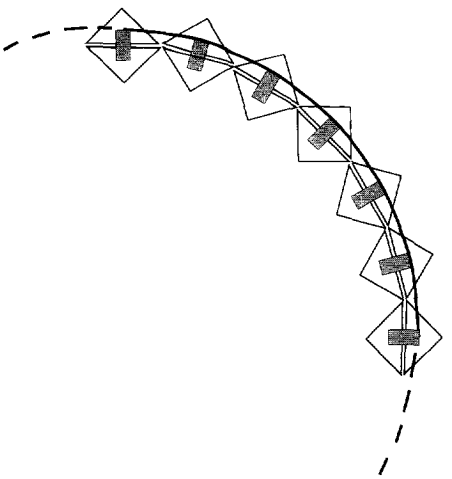

Fig. 3. The wall of the cylinder was built up of particles consisting of two triangles connected by damped beams to simulate a rough damping wall.

diameter $D = 4\,\mathrm{cm}$. The wall of the cylinder consists of particles as shown in Fig. 3 to simulate a rough damping surface. The outer triangles are fixed at the uniformly rotating ring, the inner ones obey the laws derived above (Eqs. (8)–(20)) when they undergo collisions with freely moving particles.

With the integration step $\delta t = 2 \times 10^{-5}$ s the simulation behaves numerical stable, i.e. the results do not vary when enlarging the step a few percent.

Fig. 4 shows a snapshot of the simulation with the angular velocity $\Omega = 0.2\,\mathrm{s}^{-1}$. The $N = 500$ complex particles consist each of 4 triangles connected by 8 beams. The gray scale codes for the particle velocity, black means high velocity.

The computations have been performed on a IBM 370/R6000 workstation. The total CPU time for the results presented in this paper was approximately 2100 hours.

4. Results

In our simulation we started with the angular velocity $\Omega = 0.1\,\mathrm{s}^{-1}$. As we will show below the flow of the material behaves stick–slip like for this velocity. After a relaxation time $t_r = 1.5\,\mathrm{s}$ we began to measure the interesting values. These values have been averaged over half a rotation before increasing the angular velocity by $\Delta\Omega = 0.1\,\mathrm{s}^{-1}$. After reaching the velocity $\Omega = 1.3\,\mathrm{s}^{-1}$ where the flow moves continuously we decreased the angular velocity in the same manner while measuring and averaging the interesting data. Fig. 5 shows the color encoded velocity distribution of the particles moving downwards on the surface of the material. The left figure shows the distribution for $\Omega = 0.1\,\mathrm{s}^{-1}$, the right for $\Omega = 1.3\,\mathrm{s}^{-1}$. Each horizontal line displays the values for a certain time. Time is increased from bottom to top. Red color encodes for high particle velocity, blue encodes for low velocity. The color coding is the same in the left and the

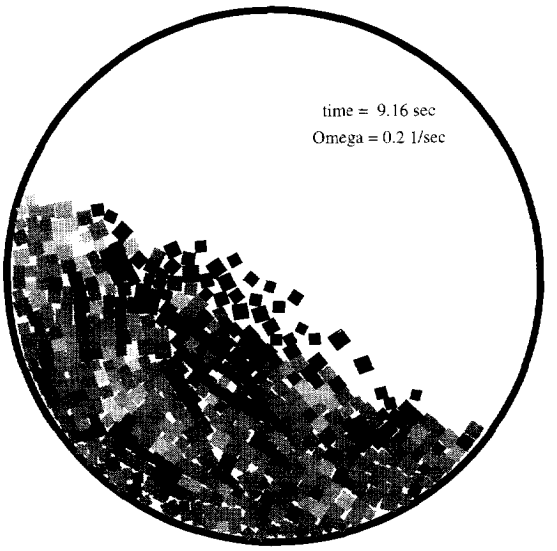

Fig. 4. Snapshot of the simulation with $N = 500$ complex particles with $P \in [0.1\,\text{cm}; 0.2\,\text{cm}]$ in a rotating cylinder with diameter $D = 4\,\text{cm}$. The angular velocity is $\Omega = 0.2\,\text{s}^{-1}$. The wall particles have not been drawn. The snapshot has been taken during an avalanche. The gray scale codes for the particle velocity.

right part of the figure. In the left part one can see that for low angular velocity the particles at the surface of the material move in a very irregular manner. One observes long periods encoded by blue color where almost no material moves downwards, sharply separated from short red regions where the material moves rapidly due to avalanches. We want to call this behavior stick–slip motion. In the equivalent figure for higher angular velocities one does not observe avalanches. The behavior is not stick–slip like but continuous in time and space.

In the natural as well as in the numerical experiment one observes avalanches. The size and the time intervals between avalanches vary irregularly. Unfortunately our numerical data are far from sufficient to calculate reliable size distributions of the avalanches.

In Fig. 6 we have drawn the averaged velocity $\langle v_s \rangle$ of the particles moving at the surface of the granular material over time (bottom figure). Each half rotation the angular velocity of the cylinder (top figure) was changed according to $\Omega = \Omega + \Delta\Omega$ while accelerating, and $\Omega = \Omega - \Delta\Omega$ while decelerating. The fluctuations become smaller since the flow is much less irregularly for larger rotation velocity. For the case of low rotation velocity one finds avalanches due to the stick–slip characteristics while for high rotation speed the flow becomes more homogeneous.

In the simulation we recorded the time series of the material flow gliding down at the surface of the granular material $f_{\rightarrow}$. When we draw the relative standard deviation

$$\sigma_{flow} = \sqrt{\frac{\overline{(\overline{f_{\rightarrow}} - f_{\rightarrow})^2}}{\overline{f_{\rightarrow}}^2}} \tag{21}$$

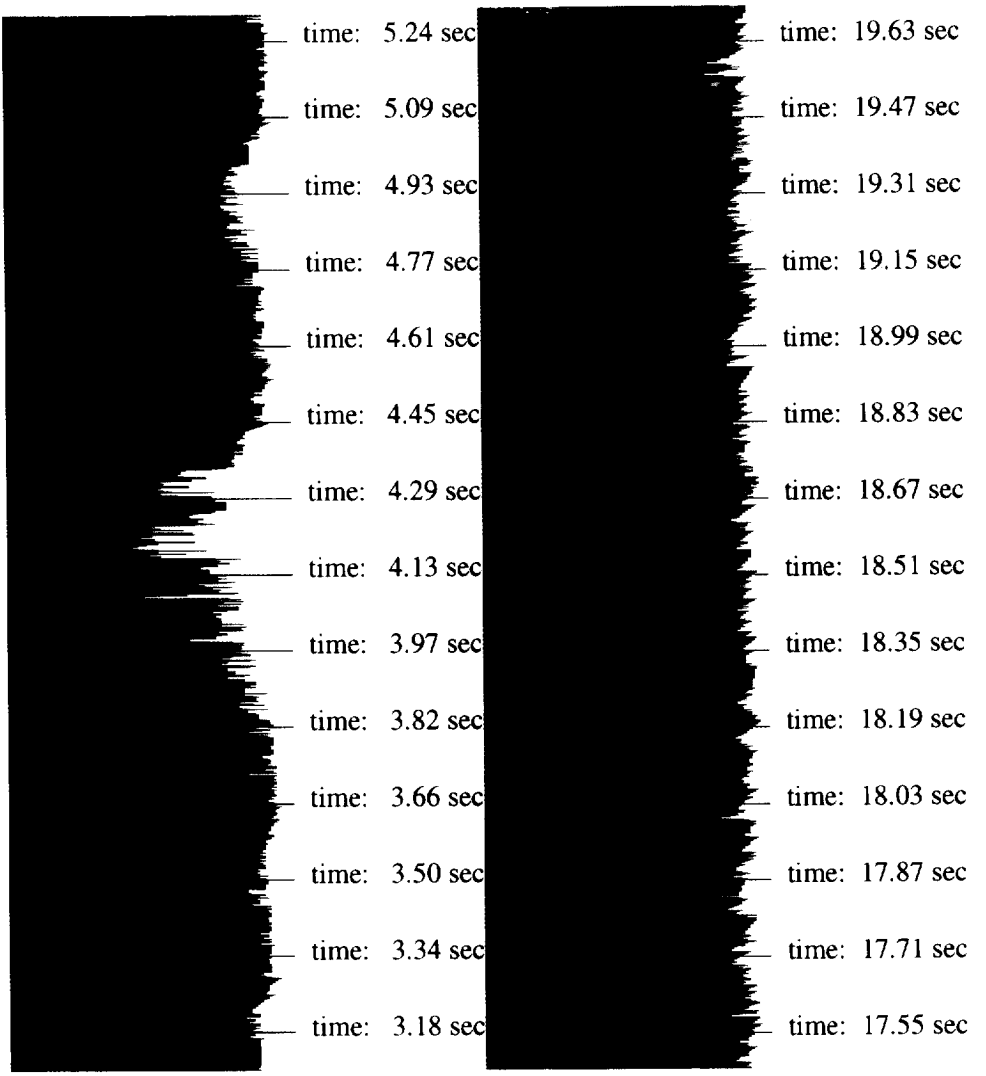

Fig. 5. The view at the surface of the moving granular material for consecutive times for $\Omega = 0.1\,s^{-1}$ (left) and $\Omega = 1.3\,s^{-1}$ (right). The colors encode for the particle velocity at the surface, red color means high velocity, blue means low velocity. Time rises from bottom to top. For low angular velocities one finds sharply distinguishable regions in space and time of different velocities which corresponds to the stick–slip like motion of the particles. The flow for $\Omega = 1.3\,s^{-1}$ is more homogeneous. The material flows from left to right in each column.

of this time series as a function of the rotation velocity Ω (Fig. 7) we find that for $\Omega > \Omega^{cr} \approx 0.6\,s^{-1}$ the relative standard deviation σ_{flow} is less than 0.1. For smaller Ω the standard deviation σ_{flow} rises dramatically due to the transition from the continuous regime to the stick–slip motion. For each value Ω we find two values σ_{flow}, one when accelerating the cylinder and one when decelerating. The dashed line in Fig. 7 connects

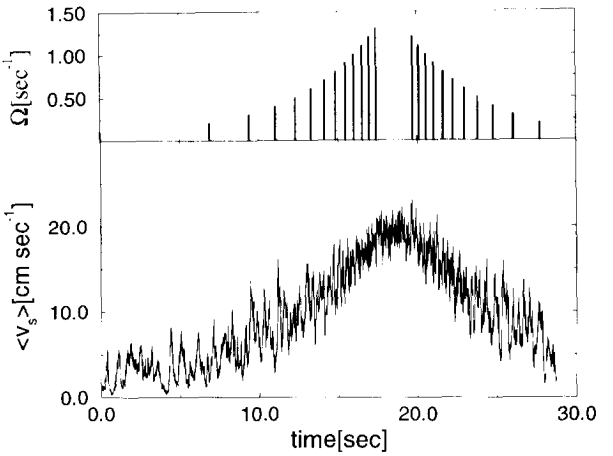

Fig. 6. The averaged positive particle velocity $\langle v_s \rangle$ over time (bottom figure). Each half rotation the angular velocity of the cylinder (top figure) was changed. For high Ω the relative fluctuations become small compared with the relative fluctuations for smaller Ω.

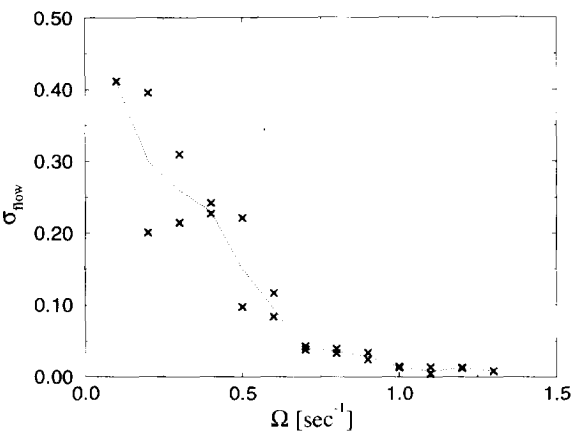

Fig. 7. The relative standard deviation (Eq. (21)) of the time series of the positive material flow in the rotating cylinder. For each Ω we measure two values σ_{flow} according to our acceleration–deceleration schedule. The dashed line connects the mean values of each of these pairs. We observe a transition between the two different flow regimes, but we are not able to determine a precise transition point. The transition takes place at the rotation velocity $\Omega \approx 0.6\,\mathrm{s}^{-1}$.

the mean values of each of these pairs.

Our acceleration–deceleration schedule was intended to reproduce the hysteresis in the critical transition point Ω^{cr} where the characteristics of the flow changes suddenly, which can be observed in the experiment [6]. When accelerating the cylinder the transition occurs at the velocity $\Omega_{\uparrow}^{cr}$ which is higher than the transition point $\Omega_{\downarrow}^{cr}$ when decelerating the cylinder. From the results presented so far we cannot observe a sharp transition between the stick–slip flow and the continuous regime as it is observed in the

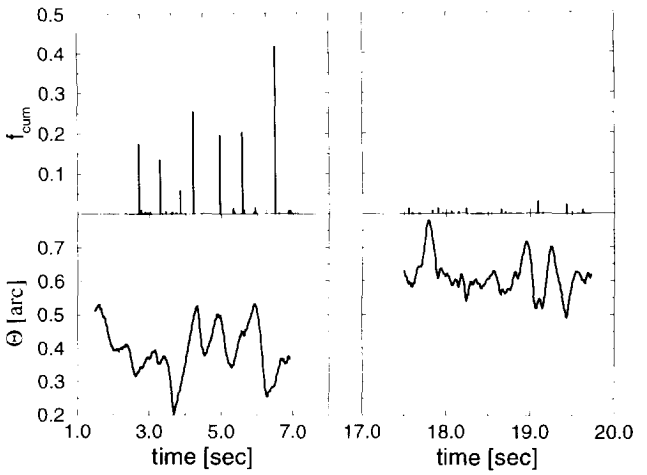

Fig. 8. Time series of the inclination Θ of the material over the time (lower figures) for the angular velocities $\Omega = 0.1\,\mathrm{s}^{-1}$ (left) and $\Omega = 1.3\,\mathrm{s}^{-1}$ (right). The values at the time axis correspond to the previous figures. In the first case the angle varies more irregularly due to avalanches. The upper figures show the material flow (explanation in the text).

experiment [6]. Hence we are not able to reproduce the hysteresis described above.

Our system is too small to provide a smooth surface to measure the inclination Θ directly. Therefore we applied an indirect method which is explained in detail in an earlier paper [19]. In Fig. 8 we have drawn the inclination Θ of the surface of the material for low angular velocity $\Omega = 0.1\,\mathrm{s}^{-1}$ (left) and for higher velocity $\Omega = 1.3\,\mathrm{s}^{-1}$ (right). The values at the time axis correspond to those in Figs. 5 and 6. In the first case the angle is smaller and varies much more irregularly due to avalanches. The mass of the material remains constant throughout the simulation. Hence the averaged flow over time in positive horizontal direction $\overline{f_{\rightarrow}}$ which is due to material flow at the surface equals the flow in negative direction $\overline{f_{\leftarrow}}$ given by the continuous material transport due to the rotation of the cylinder. The net flow $\Delta f = f_{\rightarrow} - f_{\leftarrow}$ fluctuates around zero. When the material moves stick-slip like in a clockwise rotating cylinder we expect that there are relatively rare events (avalanches) when the material moves in positive direction and time intervals, where the flow on the surface is almost zero, i.e. $\Delta f = -f_{\leftarrow}$ (see also Fig. 5). For higher rotation speed one expects that the material moves homogeneously and there are only small fluctuations of Δf. The impulses in the upper part of Fig. 8 show the cumulative positive material flow between each two consecutive times $t_i^{(\Delta f=0)}$ and $t_{i+1}^{(\Delta f=0)}$ when $\Delta f = 0$ divided by the negative flow $f_{\leftarrow}$, i.e.

$$f_{cum}\left(\frac{t_{i+1} - t_i}{2}\right) = \frac{1}{f_{\leftarrow}} \int_{t_i^{(\Delta f=0)}}^{t_{i+1}^{(\Delta f=0)}} \Delta f dt \,. \tag{22}$$

These values give a quantitative measure for the irregularity of the flow. One can see that for low Ω one observes fewer but much bigger distinguishable avalanches than for

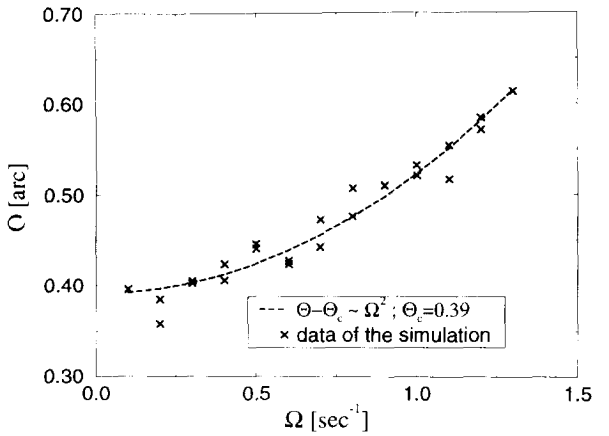

Fig. 9. The inclination Θ of the material surface over the angular velocity Ω. The dotted line displays the function which has been measured experimentally by Rajchenbach [6].

high angular velocity. For low angular velocity Ω one finds a strong correlation between avalanches (top Fig. 8) and sudden decreases of the inclination Θ (bottom figure).

The inclination of the surface of the material is a function of the angular velocity. Rajchenbach [6] determined the law experimentally to be

$$\Theta - \Theta_c \sim \Omega^2 \,, \tag{23}$$

where Ω_c is a constant. For each angular velocity Ω we measured in the simulation the inclination of the surface Θ. Fig. 9 shows the inclination Θ of the material surface over the angular velocity Ω and the function in Eq. (23). The numerical data points are located at both sides of the experimental curve. Although there are not enough data points to confirm the experimental results, we can show at least that the experimental and theoretical results do not contradict each other. The measured value for the critical angle is $\Theta_c = 22.3°$. Typical values for the experimentally measured angle of repose lie between $\Theta_c = 20°$ and $\Theta_c = 30°$, Bretz et al. for instance found $\Theta_c \approx 25°$ [34]. Values for the critical angle found in earlier simulation [19] are $\Theta_c \approx 8°$ for circular particles and $\Theta_c \approx 18°$ for non-circular compound particles [19].

5. Conclusion

We presented a model to simulate the translational and rotational movement of complex particles in a rotating drum. The particles consist of triangles connected to each other by beams. Energy dissipation is caused by inner degrees of freedom. Our model is able to predict the angle of the surface of the granular material with the horizontal line with higher accuracy than other models. The angle given by our model is in the same range as experimental values and higher than the angle predicted by models using circular disks or particles consisting of circles. We think that this advantage of the model

is caused by the use of particles with the more realistic polygonal shape which allows to take steric effects into account. One drawback of our model is its slowness which is due to the complexity of the numerical calculation. As also observed in experiments and in other simulations we found two flow regimes, a stick–slip motion of the grains for low drum frequencies and a continuous flow regime for high frequencies. Our data fit well with the power law between the surface flow and the surface angle found experimentally by Rajchenbach. Unfortunately, they are not yet sufficient to calculate the precise exponent. Further optimization and more simulation runs have to be performed.

Acknowledgements

We thank H. J. Herrmann, S. Melin, S. Schwarzer and F. Spahn for helpful discussions, and S. Seefeld for the animated visualization of the data.

References

[1] L. Rolf, Zement-Kalk-Gips 46 (1993) 117.
[2] B. Rothkegel, Örtliche Verteilung der Stoßenergien $\geq$ 22 mJ und die zugeordneten Bewegungszustände von Modellmahlkörpern in einer Modellkugelmühle (Shaker, Aachen, 1992).
[3] H. Hashimoto and R. Watanabe, in: Proc. 1st Nisshin Engineering Particle Technology International Seminar, Osaka (1993), K. Iinoya, Y. Tsuji, H. Masuda and K. Higashitani (eds.).
[4] M. Nakagawa, preprint (1993).
[5] G.R. Woodle and J.M. Munro, Powder Techn. 76 (1993) 241.
[6] J. Rajchenbach, Phys. Rev. Lett. 65 (1990) 2221.
[7] W.M. Visscher and M. Bolsterli, Nature 239 (1972) 504.
[8] R. Jullien, P. Meakin and A. Pawlovitch, Phys. Rev. Lett. 69 (1992) 640.
[9] G.C. Barker, A. Mehta and M.J. Grimson, Phys. Rev. Lett. 70 (1993) 2194.
[10] G. Baumann, E. Jobs and D.E. Wolf, in: Fractals in Natural Sciences, Budapest 1993, M. Matsuhita, M. Shlesinger and T. Vicsek (eds.) (World Scientific, Singapore, 1993).
[11] G. Baumann, I.M. Jánosi and D.E. Wolf, Europhys. Lett. 27 (1994) 203.
[12] G. Baumann, I.M. Jánosi and D.E. Wolf, Phys. Rev. E 51 (1995) 2.
[13] M.P. Allen and D.J. Tildesley, Computer Simulations of Liquids (Clarendon Press, Oxford, 1987).
[14] P.A. Cundall and O.D.L. Strack, Géotechnique 29 (1979) 47.
[15] P.K. Haff and B.T. Werner, Powder Techn. 48 (1986) 239.
[16] H. Hertz, J. f. reine u. angewandte Math. 92 (1882) 156.
[17] G.H. Ristow, Europhys. Lett. 28 (1994) 97.
[18] G.H. Ristow, F. Cantelaube-Lebec and D. Bideau, preprint (1994).
[19] T. Pöschel and V. Buchholtz, Chaos, Solitons and Fractals (in press) (1993).
[20] J.A.C. Gallas and S. Sokołowski, J. Mod. Phys. B 7 (1993) 2037.
[21] O.R. Walton and R.L. Braun, Joint DOE/NSF Workshop on flow of particulates and fluids (1993).
[22] T. Pöschel and V. Buchholtz, Phys. Rev. Lett. 71 (1993) 3963.
[23] V. Buchholtz and T. Pöschel, Physica A 202 (1994) 390.
[24] G.G. Mustoe and G. DePorter, in: Powders and Grains '93, C. Thornton (ed.) (Balkema, Rotterdam, 1993).
[25] C. Hogue and D.E. Newland, in: Powders and Grains '93, C. Thornton (ed.) (Balkema, Rotterdam, 1993).
[26] W. Stronge, Proc. Roy. Soc A 431 (1990) 169.
[27] H.-J. Tillemans and H.-J. Herrmann, preprint (1995).
[28] H.-J. Tillemans, Molekulardynamik-Simulationen beliebig geformter Teilchen, PhD thesis, University of Cologne (1994).

[29] S.P. Timoshenko and J.M. Gere, Mechanics of Materials (van Nordstrand Reinhold Company, New York, 1972).
[30] T. Pöschel and V. Buchholtz, preprint (1995).
[31] W. Form, G.A. Kohring, A. Melin, H. Puhl and H.J. Tillemans, preprint (1994).
[32] C.W. Gear, Technical Report ANL 7126, Argonne National Laboratory (1966).
[33] H.J. Herrmann, A. Hansen and S. Roux, Phys. Rev. B. 39 (1989) 637.
[34] M. Bretz, J.B. Cunningham, P.L. Kurczynski and F. Nori, Phys. Rev. Lett. 69 (1992) 2431.